Elastoplastic analysis of plane stress/strain structures via restricted basis linear programming

H. Moharrami [a,*], M.R. Mahini [b], G. Cocchetti [c]

[a] Department of Civil and Environmental Engineering, Tarbiat Modares University, Tehran, Iran
[b] Department of Civil Engineering, Persian Gulf University, Boushehr, Iran
[c] Department of Civil and Environmental Engineering, Technical University (Politecnico) of Milan, piazza L. da Vinci, 32-20133 Milan, Italy

Received 11 December 2013
Accepted 27 August 2014

1. Introduction

Analysis of structures composed of elastoplastic materials is still a growing area in the field of structural mechanics. The need for realistic responses of structures to the increasing loads (such as heavy live loads, crash loads, lateral quake/wind loads, and explosions) or need for safety assessment of structures (commonly required in limit load analysis and design procedures), have drawn attention of several researchers toward this subject [1–3].

Using piecewise-linear (PWL) yield surfaces in combination with optimization techniques has opened a new horizon of study known as PWL elastoplasticity [4]. Mathematical programming (MP) has been employed by several researchers in nonlinear analysis of structures and has found to be a very robust and versatile approach to solution of problems of this kind. MP based approaches do not contain the difficulties of the iterative approaches such as the implementation of cumbersome return algorithms, the enforcing of convergence criteria, and so on. Satisfying the yield and equilibrium equations at global scale, unconditional stability (that appears in step-by-step solution schemes) and use of easily coded optimization algorithms (frequently available in commercial software) are encouraging features of such approaches that motivate researches in this area. In the following, the history of such approaches is cited briefly.

Mathematical linear programming has been considered for rigid-plastic limit analysis (LA) of framed structures and its historical and theoretical background has been deeply discussed and demon-strated in many nonlinear analysis text books, e.g. see [5]. Maier [6,7] proposed the use of quadratic programming (QP) in elastoplas-tic analyses and derived a matrix formulation for framed structures governed by PWL constitutive models [8]. The use of linear comple-mentarity problem (LCP) solvers was also found to be efficient and a restricted basis linear programming (RBLP) was proposed as an alternative to QP [9]. Therefore LCP concept was extended to various engineering problems such as dynamic analysis [10], shakedown analysis [11], and softening frames [12,13]. Also some researchers dealt with piecewise-linearization of yield surfaces, so as to be uti-lized in optimization approaches as linear constraints [14–16]. Recently a modified version of RBLP has been proposed in the spirit of framed structures, which automatically captures and handles any local unloading and removes any need for sub-problem solution in the cases of reaching yield surface corners [17,18]. This approach has been successfully used in elastoplastic analysis of softening frames and the proposed maximization criterion has shown an excellent capability in capturing the exact response of structures. This approach, which basically works in an incremental manner, preserves the distinct features of the step-by-step method, namely exactness and unconditional stability, while removes its disadvan-tages addressed in [12].

* Corresponding author. Telefax: +98 21 82883324.
E-mail addresses: hamid@modares.ac.ir (H. Moharrami), mahini@pgu.ac.ir (M.R. Mahini), giuseppe.cocchetti@polimi.it (G. Cocchetti).

In spite of pervasive studies on MP approaches applied to skeletal structure analyses, which have made this topic a well-developed area, it has been rarely utilized in direct analysis of plane stress/strain problems. Kaliszky and Lógó [19] presented a mixed variational principle for plane-strain problems characterized by bilinear hardening materials. In this approach the load multiplier is maximized using nonlinear MP solvers in the view of nonlinear nature of constraints. Another development in MP approaches toward 2D-stress/strain problems has appeared in [20], where traditional Mohr–Coulomb yield surface is piecewise-linearized and used for safety assessment by load factor maximization. Utilizing this approach, which is efficiently improved by the aid of sifting and re-meshing techniques, the holonomic response of structures and corresponding limit load are detected with a reasonable accuracy.

The most recent contribution to direct elastoplastic analysis of plane stress and plane strain structures by the aid of optimization tools is the complementarity approach proposed by Tanga-ramvong et al. [21]. This approach implements a mixed finite element formulation, developed by Capsoni and Corradi for quad-rilateral bilinear elements [22,23], in constructing an MP problem. As for constraints, the von Mises or Tresca yield criteria are considered in their original nonlinear forms. The resulted MP is solved using an industry-standard complementarity solver GAMS/PATH with an interface for MATLAB environment. This approach belongs to holonomic solution category and sufficiently small load steps are needed to reduce the amount of errors appearing due to possible local unloadings. In this approach a relatively large frac-tion of the CPU time (27–82% in some studied structures) is spent for load estimations beyond the limit load, i.e. infeasible load steps.

In this paper, the RBLP is extended to 2D-Stress/Strain problems following a similar approach discussed in [17,18]. To this end, theoretical aspects of problem including: field approximation, piecewise-linearization of von Mises yield model in 2D-stress/strain, and development of linear mixed hardening constitutive laws are presented in Section 2. Formulation of the problem and its implementation in the MP problem are explained in Section 3. In Section 4, the solution procedure of the mathematical programming problem is discussed and finally, in Section 5, some numerical examples are presented to demonstrate the capabilities of the proposed algorithm and numerically validate its results.

Bold-face, regular, and italic symbols are adopted herein for matrices, vectors and scalars, respectively. Superscript T means transpose, and dots stand for rates (i.e. derivative with respect to ordering, not necessarily physical, time).

2. Theoretical formulation

2.1. Field approximations

It is well-known that in LA by popular FEM the computed safety factor might severely be affected by locking, see e.g. [24]. Herein a multi-field mixed discretization is adopted: the pairs of conjugate variables are modeled and the conservation of the scalar product for conjugate fields is imposed in a weak form. In such approaches, the discrete problem is formulated in terms of generalized variables and using appropriate shape functions, which lets to rule out the shear locking phenomena by relaxing the kinematic constraints that induce locking. The theoretical aspects of mixed for-mulation is deeply studied in literature, see e.g. [25–27], and are not brought here for the sake of brevity. In this study, quadrilateral elements are considered and the displacement field, $u_e(\xi, \eta)$, within the element e is approximated by quadratic isoparametric shape functions, $\mathbf{N}$, in the space of natural coordinates (ξ, η), and with reference to the nodal displacements U_e:

$$u_e(\xi,\eta) = \mathbf{N}U_e \tag{1}$$

Four Gauss points, $g = 1$–4, over each element are used for numerical integration and the stress and strain fields are assumed to vary linearly over the element. Herein the actual stress components corresponding to the Gauss points are assumed as the element generalized stress, $\bar{\sigma}_e$, and bilinear shape functions, $\mathbf{\Psi}^e_\sigma$, which are referring to the Gauss points instead of element nodes, are used to interpolate stresses, $\sigma_e(\xi,\eta) = [\,\sigma_x(\xi,\eta),\ \ \sigma_y(\xi,\eta),\ \ \tau_{xy}(\xi,\eta)]^T_e$, over the element:

$$\sigma_e(\xi,\eta) = \mathbf{\Psi}^e_\sigma \bar{\sigma}_e \tag{2}$$

Note that the (3×12) stress shape function matrix, once computed at the gth Gauss point, collects three zero blocks and an identity matrix $\mathbf{I}_{3\times3}$, located at the block corresponding to the considered Gauss point, e.g. for $g = 1$:

$$\mathbf{\Psi}^e_\sigma\big|_{g=1} = [\,\mathbf{I}_{3\times3} \quad \mathbf{0}_{3\times3} \quad \mathbf{0}_{3\times3} \quad \mathbf{0}_{3\times3}\,] \tag{3}$$

Also the strain field $\varepsilon_e(\xi,\eta) = [\,\varepsilon_x(\xi,\eta),\ \ \varepsilon_y(\xi,\eta),\ \ \gamma_{xy}(\xi,\eta)]^T_e$, within the element, is approximated by the shape functions $\mathbf{\Psi}^e_\varepsilon$ and governed by the element generalized strain vector $\bar{\varepsilon}_e$ as follows:

$$\varepsilon_e(\xi,\eta) = \mathbf{\Psi}^e_\varepsilon \bar{\varepsilon}_e \tag{4}$$

In order to preserve the scalar product of conjugate quantities in terms of actual model variables and the generalized ones, the strain field shape function over the element domain Ω is selected as follows:

$$\mathbf{\Psi}^e_\varepsilon = \mathbf{\Psi}^e_\sigma \left(\int_\Omega \mathbf{\Psi}^{e^T}_\sigma \mathbf{\Psi}^e_\sigma d\Omega \right)^{-1} \tag{5}$$

Also this shape function (3×12) matrix, once computed at the gth Gauss point, collects three zero blocks and a scaled identity matrix. The scale factor is $(tJ_g)^{-1}$ wherein t is the element thickness and J_g is the Jacobian matrix determinant, calculated at the Gauss point g. For instance, at the first Gauss point $(g = 1)$ the strain shape function matrix becomes:

$$\mathbf{\Psi}^e_\varepsilon\big|_{g=1} = \left[\tfrac{1}{tJ_{g=1}} \mathbf{I}_{3\times3} \quad \mathbf{0}_{3\times3} \quad \mathbf{0}_{3\times3} \quad \mathbf{0}_{3\times3} \right] \tag{6}$$

By weighting the strain definition relation, the consistency matrix $\mathbf{C}_e$ for linear kinematics is determined as:

$$\mathbf{C}_e = \int_\Omega \mathbf{\Psi}^{e^T}_\varepsilon \nabla \mathbf{N} d\Omega \tag{7}$$

wherein, ∇ is the well-known symmetric gradient operator, generating the local strain field from the displacement field. The consistency matrix $\mathbf{C}_e$, the nodal displacements U_e and the nodal forces f_e can be related to the generalized stresses and strains by the following relations:

$$\begin{aligned} \bar{\varepsilon}_e &= \mathbf{C}_e U_e \\ f_e &= \mathbf{C}^T_e \bar{\sigma}_e \end{aligned} \tag{8}$$

Accordingly, the element stiffness matrix reads:

$$\mathbf{K}_e = \mathbf{C}^T_e \overline{\mathbf{D}}_e \mathbf{C}_e \tag{9}$$

wherein the generalized material stiffness matrix $\overline{\mathbf{D}}_e$ is evaluated in terms of material constitutive stiffness matrix $\mathbf{D}_e$ and strain shape functions through the following integral:

$$\overline{\mathbf{D}}_e = \int_\Omega \mathbf{\Psi}^{e^T}_\varepsilon \mathbf{D}_e \mathbf{\Psi}^e_\varepsilon d\Omega \tag{10}$$

The material constitutive stiffness matrix, which is defined in terms of the Young modulus E and Poisson's ratio ν, assumes different forms for plane stress and plane strain cases:

$$\mathbf{D}_e = \frac{E}{1-\nu^2}\begin{bmatrix} 1 & \nu & 0 \\ \nu & 1 & 0 \\ 0 & 0 & (1-\nu)/2 \end{bmatrix} \quad \text{(plane stress)}$$

$$\mathbf{D}_e = \frac{E}{(1+\nu)(1-2\nu)}\begin{bmatrix} 1-\nu & \nu & 0 \\ \nu & 1-\nu & 0 \\ 0 & 0 & (1-2\nu)/2 \end{bmatrix} \quad \text{(plane strain)} \tag{11}$$

Finally, the element generalized plastic multipliers $\bar{\lambda}_e$ are referred to the Gauss points and are assumed to govern the modeled local plastic multipliers λ_e by the above bilinear shape functions:

$$\lambda_e(\xi,\eta) = \mathbf{\Psi}^e_{\lambda}\bar{\lambda}_e, \quad \mathbf{\Psi}^e_{\lambda} = \mathbf{\Psi}^e_{\sigma} \tag{12}$$

2.2. On piecewise linearization of elastic–plastic J_2 model

One of the most popular and well-known yield criteria is the one proposed by von Mises, also known as J_2 plasticity model, and has been found in adequate accuracy for classical metal plas-ticity problems including: crash analysis, metal forming and gen-eral collapse studies in relatively low temperatures [28,29]. In this study, this yield criterion is used with associative plasticity. The key point in nonlinear analysis via RBLP is to develop a PWL yield criterion in a matrix form. This has been considered as the main subject of this Subsection. Von Mises yield domain, for an iso-tropic material, is defined in terms of second deviatoric stress invariant J_2 as follows:

$$F = \sqrt{3J_2} - \sigma_0 \leqslant 0 \tag{13}$$

where σ_0 is the material yield limit; for a generic stress state, i.e. 3D-stress state, J_2 can be computed in terms of stress components to obtain the following expanded form:

$$F = \sqrt{\sigma_x^2+\sigma_y^2+\sigma_z^2-\sigma_x\sigma_y-\sigma_y\sigma_z-\sigma_z\sigma_x+3\tau_{xy}^2+3\tau_{yz}^2+3\tau_{zx}^2} - \sigma_0 \leqslant 0 \tag{14}$$

In the above definition σ_i and τ_{ij} are referring to normal and shearing stress components, respectively. For the piece-wise linearization of the yield function, it results more convenient to normalize stress components with respect to material yield stress, i.e. $\underline{\sigma}_i = \sigma_i/\sigma_0$ and $\underline{\tau}_{ij} = \tau_{ij}/\sigma_0$, to obtain:

$$F = \sqrt{\underline{\sigma}_x^2+\underline{\sigma}_y^2+\underline{\sigma}_z^2-\underline{\sigma}_x\underline{\sigma}_y-\underline{\sigma}_y\underline{\sigma}_z-\underline{\sigma}_z\underline{\sigma}_x+3\underline{\tau}_{xy}^2+3\underline{\tau}_{yz}^2+3\underline{\tau}_{zx}^2} - 1 \leqslant 0 \tag{15}$$

Geometrical interpretation of such yield locus is a cylindrical shell with axis coinciding with $\underline{\sigma}_x = \underline{\sigma}_y = \underline{\sigma}_z$ line in the space of principal stresses. The J_2 yield model, Eq. (15), in σ_x–σ_y plane stress mode, i.e. $\sigma_z = \tau_{yz} = \tau_{zx} = 0$, reduces to:

$$f = \underline{\sigma}_x^2 + \underline{\sigma}_y^2 - \underline{\sigma}_x\underline{\sigma}_y + 3\underline{\tau}_{xy}^2 - 1 \leqslant 0 \tag{16}$$

The geometrical description of such a yield locus is an ellipsoid in $\underline{\sigma}_x$–$\underline{\sigma}_y$–$\underline{\tau}_{xy}$ space and an oblique oval in $\underline{\tau}_{xy} = 0$ plane as shown in Fig. 1. Herein the aim is to linearize the yield surface with adjustable accuracy, i.e. controllable number of yield planes, which will provide a suitable tool beside the sifting technique.

To this end, two sets of perpendicular planes are assumed in $\underline{\sigma}_x$–$\underline{\sigma}_y$–$\underline{\tau}_{xy}$ stress space, and used to locate the desired discretizing points on the yield surface:

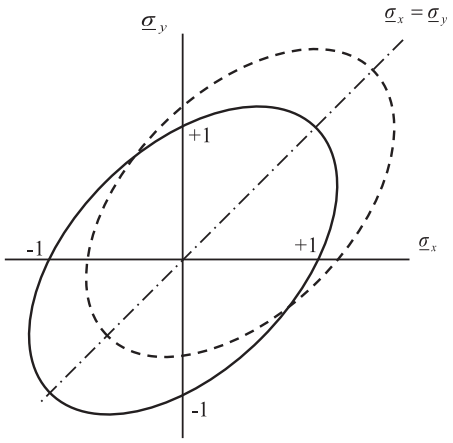

Fig. 1. von Mises yield locus in plane stress (solid line) and plane strain (dotted line) in the plane $\underline{\tau}_{xy} = 0$.

"*Transversal subdividing planes*"; which is the set of planes perpendicular to the diagonal $\underline{\sigma}_x = \underline{\sigma}_y$.

Such planes are generally expressed in the form $\underline{\sigma}_x + \underline{\sigma}_y = \xi_i$, in which ξ_i is referred to as transversal discretizing parameter and is limited to $-2 \leqslant \xi_i \leqslant +2$ in order to prevent null intersection with the oval depicted in Fig. 1.

"*Radial subdividing planes*"; which is the set of planes passing through the diagonal $\underline{\sigma}_x = \underline{\sigma}_y$ and forming an angle θ_j with the $\tau_{xy} = 0$ plane. This group of planes can be given the following mathematical description $(\underline{\sigma}_x - \underline{\sigma}_y)\tan\theta_j - 2\underline{\tau}_{xy} = 0$, in which θ_j is defined as radial discretizing parameter and is limited to $0 \leqslant \theta_j \leqslant 2\pi$.

By intersecting these two planes with the yield surface $f = 0$, Eq. (16), the coordinates of the discretizing points, $[\hat{\sigma}_x, \hat{\sigma}_y, \hat{\tau}_{xy}]$, are found to be as follows:

$$\begin{aligned} \hat{\sigma}_x &= \frac{\xi_i}{2} + \frac{\cos\theta_j}{2}\sqrt{\frac{4-\xi_i^2}{3(1+\sin^2\theta_j)}} \\ \hat{\sigma}_y &= \frac{\xi_i}{2} - \frac{\cos\theta_j}{2}\sqrt{\frac{4-\xi_i^2}{3(1+\sin^2\theta_j)}} \\ \hat{\tau}_{xy} &= \frac{\sqrt{2}\sin\theta_j}{2}\sqrt{\frac{4-\xi_i^2}{3(1+\sin^2\theta_j)}} \end{aligned} \tag{17}$$

The normal vector to the yield locus at the generic discretizing point reads:

$$\left.\frac{\partial f}{\partial\sigma}\right|_{\hat{\sigma}} = \frac{1}{\sigma_0}\begin{Bmatrix} 2\hat{\sigma}_x - \hat{\sigma}_y \\ 2\hat{\sigma}_y - \hat{\sigma}_x \\ 6\hat{\tau}_{xy} \end{Bmatrix} = \frac{1}{\sigma_0}\begin{Bmatrix} \frac{\xi_i}{2} + \frac{3\cos\theta_j}{2}\sqrt{\frac{4-\xi_i^2}{3(1+\sin^2\theta_j)}} \\ \frac{\xi_i}{2} - \frac{3\cos\theta_j}{2}\sqrt{\frac{4-\xi_i^2}{3(1+\sin^2\theta_j)}} \\ 3\sqrt{2}\sin\theta_j\sqrt{\frac{4-\xi_i^2}{3(1+\sin^2\theta_j)}} \end{Bmatrix} \tag{18}$$

Finally, having the discretizing point coordinates, Eq. (17), and the normal vector Eq. (18), equation of the corresponding yield plane is simply determined:

$$\begin{aligned} f_{ij} = {} & \frac{1}{4}\left(\xi_i + 3\cos\theta_j\sqrt{\frac{4-\xi_i^2}{3(1+\sin^2\theta_j)}}\right)\underline{\sigma}_x \\ & + \frac{1}{4}\left(\xi_i - 3\cos\theta_j\sqrt{\frac{4-\xi_i^2}{3(1+\sin^2\theta_j)}}\right)\underline{\sigma}_y \\ & + \frac{3\sqrt{2}}{2}\left(\sin\theta_j\sqrt{\frac{4-\xi_i^2}{3(1+\sin^2\theta_j)}}\right)\underline{\tau}_{xy} - 1 = 0 \end{aligned} \tag{19}$$

From the above set of yield planes, defined at any Gauss point g, the piece-wise linearization of the yield surface can be given the following matrix notation:

$$Y_g = \mathbf{\Phi}_g^T \sigma_g - \{1\} \leqslant 0 \tag{20}$$

where $\mathbf{\Phi}_g$ and σ_g are the yield matrix and the stress vector corresponding to the Gauss point g, respectively, considered as follows:

$$\mathbf{\Phi}_g = \begin{bmatrix} \frac{1}{4}\left(\xi_i + 3\cos\theta_j \sqrt{\frac{4-\xi_i^2}{3(1+\sin^2\theta_j)}}\right) \\ \frac{1}{4}\left(\xi_i - 3\cos\theta_j \sqrt{\frac{4-\xi_i^2}{3(1+\sin^2\theta_j)}}\right) \\ \frac{3\sqrt{2}}{2}\left(\sin\theta_j \sqrt{\frac{4-\xi_i^2}{3(1+\sin^2\theta_j)}}\right) \end{bmatrix}_{3\times m} \tag{21}$$

$$\sigma_g = \begin{Bmatrix} \underline{\sigma}_x \\ \underline{\sigma}_y \\ \underline{\tau}_{xy} \end{Bmatrix}_g$$

In the above formula m is the number of yield planes used to approximate the original yield surface. It is obvious that the proposed linearization represents an external delimitation of the original yield surface and upper bounds on the collapse load are expected; however, for reasonably fine discretizations, these approximations will bring the results close to the exact ones. Otherwise, the piecewise linear domain can be homothetically scaled to get an internal (i.e. safe) delimitation to the original yield surface.

Using the proposed PWL version of von Mises yield surface, one can control the accuracy of linearization by selecting suitable number of subdivisions over θ and ξ domains. To this purpose, one choice is to express the radial control parameter by $\theta_j = 2\pi j/M$, in which M represents the number of radial subdivisions and j runs from 1 to M. Also the transversal controlling parameter can be selected from any desirable distribution over $[-2, +2]$ interval. This feature will provide a very suitable tool to have a more accurate approximation around the predicted stress state at any Gauss point, if needed. A 3D plot of the suggested PWL yield surface, formed by 222 yield planes, can be found in Fig. 2 for $\xi = [0, \pm0.5, \pm1, \pm1.2, \pm1.7, \pm1.9, \pm2]$ and $M = 20$.

2.3. Hardening PWL constitutive model for plane stress and plane strain problems

The obtained PWL yield surface, Eq. (20), has been derived for a plane stress mode; it can be easily converted to plane strain mode according to the following consideration. The elastic constitutive equations for a plane strain mode can be expressed as:

$$\sigma_g = \mathbf{B}^T \left(\begin{Bmatrix} \underline{\sigma}_x \\ \underline{\sigma}_y \\ \underline{\tau}_{xy} \end{Bmatrix}_g - \frac{E}{(1-2\nu)^2} \mathbf{\Gamma} P_g \right) \tag{22}$$

where $\mathbf{B} = \mathbf{I}_{3\times3} - \nu\mathbf{\Gamma}$ and the in-plane equivalent plastic strains, P_g, and $\mathbf{\Gamma}$ have the following definitions:

$$P_g = \begin{Bmatrix} \varepsilon_x^p + \nu\varepsilon_z^p \\ \varepsilon_y^p + \nu\varepsilon_z^p \\ \gamma_{xy} \end{Bmatrix}_g, \quad \mathbf{\Gamma} = \begin{bmatrix} 1 & 1 & 0 \\ 1 & 1 & 0 \\ 0 & 0 & 0 \end{bmatrix}, \tag{23}$$

It can be easily verified that the in-plane plastic strain vector $\varepsilon_g^p = [\,\varepsilon_x^p \quad \varepsilon_y^p \quad \gamma_{xy}^p\,]_g^T$ can be expressed in terms of in-plane equivalent plastic strain vector P_g by the following formulas:

$$\varepsilon_g^p = \mathbf{A} P_g, \quad \mathbf{A} = \frac{1}{1-2\nu} \begin{bmatrix} 1-\nu & \nu & 0 \\ \nu & 1-\nu & 0 \\ 0 & 0 & 1-2\nu \end{bmatrix} \tag{24}$$

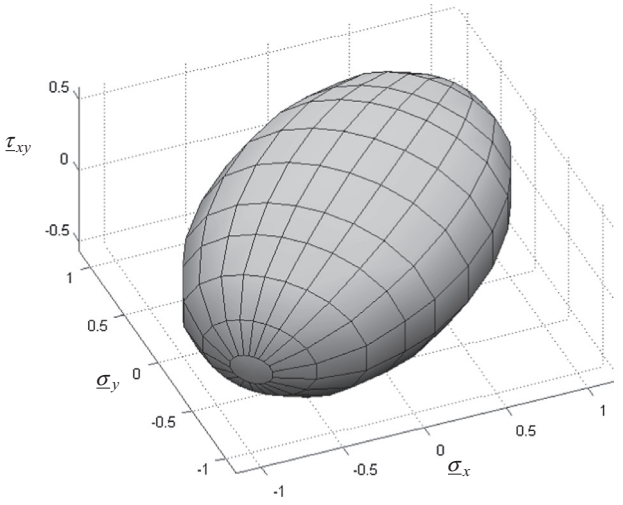

Fig. 2. Piece-wise linear approximation ($M = 20$ and $\xi = [0, \pm0.5, \pm1, \pm1.2, \pm1.7, \pm1.9, \pm2]$) of the von Mises ellipsoid in 2D-Stress mode. The plot is also valid for 2D-Strain mode provided that $\underline{\sigma}_z = 0$ is assumed.

It results that the plane stress yield conditions, Eq. (20), can be easily converted to the plane strain ones, by modifying the yield matrix $\mathbf{\Phi}_g$ using the $\mathbf{B}$ matrix and considering the term $E\mathbf{\Gamma}P_g/(1-2\nu)^2$ as a part of the back stress vector, reflecting the fictitious hardening of plane strain problems (see e.g. [30]). In order to develop a unified and more general formulation, the PWL yield condition Eq. (20) is written in the following form:

$$Y_g = \hat{\mathbf{\Phi}}_g^T(\sigma_g - \alpha_g) - \beta_g - \{1\} \leqslant 0 \tag{25}$$

where $\hat{\mathbf{\Phi}}_g$ is the yield matrix relevant to the problem state, i.e. $\hat{\mathbf{\Phi}}_g = \mathbf{\Phi}_g$ for plane stress and $\hat{\mathbf{\Phi}}_g = \mathbf{B}\mathbf{\Phi}_g$ for plane strain; α_g is the back stress vector accounting for kinematic hardening by controlling the position of the yield locus, which contains also the term $E\mathbf{\Gamma}P_g/(1-2\nu)^2$ for plane strain problems (see below); and β_g is a vector that accounts for isotropic hardening by controlling the size of yield locus. For the plane stress problems, P_g coincides with ε_g^p, namely $\mathbf{A}$ has to be replaced by an identity matrix.

For the whole element, here considered with a quadrilateral shape, quadratic displacements (Q8) with four Gauss points, it is custom to weight the yield condition Eq. (25) with bilinear shape functions $\mathbf{\Psi}_\lambda^e$, and to integrate the weighted expression over the element domain Ω. This will return the original yield constraints, relevant to the Gauss points separately, scaled by the factor tJ_g. Then, the multiplying coefficients can be easily removed to go back to the original yield conditions introduced by Eq. (25) separately for each Gauss point. As a result, the yield condition Eq. (25), which is defined at Gauss point level, can be simply rewritten at the element level as follows:

$$Y_e = \hat{\mathbf{\Phi}}_e^T(\mathbf{\Psi}_\sigma^{e*}\bar{\sigma}_e - \alpha_e) - \beta_e - \{1\} \leqslant 0 \tag{26}$$

where

$$\hat{\mathbf{\Phi}}_e = \begin{bmatrix} \hat{\mathbf{\Phi}}_{g=1} & & & \\ & \hat{\mathbf{\Phi}}_{g=2} & & \\ & & \hat{\mathbf{\Phi}}_{g=3} & \\ & & & \hat{\mathbf{\Phi}}_{g=4} \end{bmatrix}, \quad \bar{\sigma}_e = \begin{Bmatrix} \bar{\sigma}_{g=1} \\ \bar{\sigma}_{g=2} \\ \bar{\sigma}_{g=3} \\ \bar{\sigma}_{g=4} \end{Bmatrix}, \quad \mathbf{\Psi}_\sigma^{e*} = \begin{bmatrix} \mathbf{\Psi}_\sigma^e\big|_{g=1} \\ \mathbf{\Psi}_\sigma^e\big|_{g=2} \\ \mathbf{\Psi}_\sigma^e\big|_{g=3} \\ \mathbf{\Psi}_\sigma^e\big|_{g=4} \end{bmatrix} = \mathbf{I}_{12\times12} \tag{27}$$

In the same manner, strain shape functions are collected in a new block-diagonal matrix, defined as follows:

$$\boldsymbol{\Psi}_{\varepsilon}^{e*} = \begin{bmatrix} \boldsymbol{\Psi}_{\varepsilon}^{e}\big|_{g=1} \\ \boldsymbol{\Psi}_{\varepsilon}^{e}\big|_{g=2} \\ \boldsymbol{\Psi}_{\varepsilon}^{e}\big|_{g=3} \\ \boldsymbol{\Psi}_{\varepsilon}^{e}\big|_{g=4} \end{bmatrix} = \begin{bmatrix} \frac{1}{J_{g=1}}\mathbf{I}_{3\times3} & & & \\ & \frac{1}{J_{g=2}}\mathbf{I}_{3\times3} & & \\ & & \frac{1}{J_{g=3}}\mathbf{I}_{3\times3} & \\ & & & \frac{1}{J_{g=4}}\mathbf{I}_{3\times3} \end{bmatrix} \tag{28}$$

Here, definitions similar to those proposed by Capsoni and Corradi [22] are adopted to define hardening parameters, α_g and β_g:

$$\begin{aligned} \alpha_e &= h_k[\cdots\bar{\bar{\Gamma}}\cdots]P_e \quad \text{(plane stress)} \\ \alpha_e &= \left(\frac{1}{2}h_k[\cdots\bar{\Gamma}\cdots] + \frac{E(1-2\nu)+\frac{3}{2}h_k}{(1-2\nu)^3}[\cdots\boldsymbol{\Gamma}\cdots]\right)P_e \quad \text{(plane strain)} \\ \beta_g &= h_i\lambda_e \end{aligned} \tag{29}$$

where h_i and h_k are the isotropic and kinematic hardening coefficients, respectively, and λ_e is the element plastic multiplier vector which collects all the plastic multipliers, ordered for all Gauss points. Also, $\bar{\Gamma}$ and $\bar{\bar{\Gamma}}$ are given the following definitions:

$$\bar{\Gamma} = \begin{bmatrix} 1 & -1 & 0 \\ -1 & 1 & 0 \\ 0 & 0 & 0 \end{bmatrix}, \quad \bar{\bar{\Gamma}} = \begin{bmatrix} 1 & 0 & 0 \\ 0 & 1 & 0 \\ 0 & 0 & \frac{1}{2} \end{bmatrix}, \tag{30}$$

Noting that $P_e = \boldsymbol{\Psi}_{\varepsilon}^{e*}\boldsymbol{\Psi}_{\sigma}^{e*T}\hat{\boldsymbol{\Phi}}_e\lambda_e$, the yield conditions at element level can be considered in the following standard form:

$$Y_e = \hat{\boldsymbol{\Phi}}_e^T\boldsymbol{\Psi}_{\sigma}^{e*}\bar{\sigma}_e - \mathbf{H}_e\lambda_e - \{1\} \leqslant 0 \tag{31}$$

where the element hardening matrix $\mathbf{H}_e$ has one of the following definitions, depending on the problem state:

$$\begin{aligned} \mathbf{H}_e &= h_k[\cdots\bar{\bar{\Gamma}}\cdots]\boldsymbol{\Psi}_{\varepsilon}^{e*}\boldsymbol{\Psi}_{\sigma}^{e*T}\hat{\boldsymbol{\Phi}}_e + h_i\mathbf{I} \quad \text{(plane stress)} \\ \mathbf{H}_e &= \left(\frac{1}{2}h_k[\cdots\bar{\Gamma}\cdots] + \frac{E(1-2\nu)+\frac{3}{2}h_k}{(1-2\nu)^3}[\cdots\boldsymbol{\Gamma}\cdots]\right)\boldsymbol{\Psi}_{\varepsilon}^{e*}\boldsymbol{\Psi}_{\sigma}^{e*T}\boldsymbol{\Phi}_e + h_i\mathbf{I} \quad \text{(plane strain)} \end{aligned} \tag{32}$$

3. Mathematical programming formulation

In order to setup the whole structural domain and formulate the mathematical programming problem, yield constraints have to be expressed for the entire structure using matrix notation. This is simply done by assembling the resulted matrices at element level. For example the yield conditions for all n_e elements can be collected in the compact form:

$$Y = \widehat{\boldsymbol{\Phi}}^T\boldsymbol{\Psi}_{\sigma}^{*}\bar{\sigma} - \mathbf{H}\lambda - \{1\} \leqslant 0 \tag{33}$$

In the above formula, $\widehat{\boldsymbol{\Phi}}$ is the global yield matrix which collects $\widehat{\boldsymbol{\Phi}}_e$ matrices in block diagonal form. $\mathbf{H}$ and $\boldsymbol{\Psi}_{\sigma}^{*}$ are also constructed in a similar manner using $\mathbf{H}_e$ and $\boldsymbol{\Psi}_{\sigma}^{e*}$, respectively. Also λ is a vector in which plastic multipliers for all elements, λ_e, are kept in order, and after all $\bar{\sigma}$ is the generalized stress vector of the whole structure composed of the elements' generalized stress vectors, $\bar{\sigma}_e$.

The generalized stress vector $\bar{\sigma}$ can be decomposed in two parts; first the elastic stress vector $\bar{\sigma}^i$, computed by a linear elastic analysis of the structure under the current level of external actions, and second one the residual stress vector $\bar{\sigma}^{ii}$ which reflects the effects of plasticity occurrence at any point over the whole domain:

$$\bar{\sigma} = \bar{\sigma}^i + \bar{\sigma}^{ii} = \mu\bar{\sigma}^0 + \bar{\boldsymbol{\sigma}}^{\nu}\bar{\varepsilon} \tag{34}$$

In the above formula, $\bar{\sigma}^0$ is the generalized stress response of the linear elastic structure to the external actions amplified by a unit factor, and μ is the external load multiplier. Also each column of the influence matrix $\bar{\boldsymbol{\sigma}}^{\nu}$ is carried out from a linear elastic analysis of the structure by considering a unit virtual generalized strain (corresponding to each generalized stress component at the Gauss points) as the exciting agent. It is worth noting that such analyses are done using the initial stiffness matrix constructed and inverted just once for the linear elastic analysis, thus the computational effort devoted to calculating the influence matrix is negligible.

Following an associated flow rule, the generalized plastic strain vector $\bar{\varepsilon}$ can be expressed in terms of stress shape functions, yield matrix, and the vector of plastic multipliers as follows:

$$\bar{\varepsilon} = \frac{\partial\mathbf{Y}}{\partial\bar{\sigma}}\lambda = \boldsymbol{\Psi}_{\sigma}^{*T}\hat{\boldsymbol{\Phi}}\lambda \tag{35}$$

Substituting Eq. (35) into (34) and afterwards in the yield conditions, Eq. (33), it results:

$$Y = (\widehat{\boldsymbol{\Phi}}^T\boldsymbol{\Psi}_{\sigma}^{*}\bar{\boldsymbol{\sigma}}^{\nu}\boldsymbol{\Psi}_{\sigma}^{*T}\widehat{\boldsymbol{\Phi}} - \mathbf{H})\lambda + \mu\widehat{\boldsymbol{\Phi}}^T\boldsymbol{\Psi}_{\sigma}^{*}\bar{\sigma}^0 - \{1\} \leqslant 0 \tag{36}$$

and, after all, a mathematical programming problem can be easily formulated as follows:

$$\begin{cases} max.\ \{1\}^T\dot{\lambda} \\ S.t.: \\ \qquad Y = (\widehat{\boldsymbol{\Phi}}^T\boldsymbol{\Psi}_{\sigma}^{*}\bar{\boldsymbol{\sigma}}^{\nu}\boldsymbol{\Psi}_{\sigma}^{*T}\widehat{\boldsymbol{\Phi}} - \mathbf{H})\lambda + \mu\widehat{\boldsymbol{\Phi}}^T\boldsymbol{\Psi}_{\sigma}^{*}\bar{\sigma}^0 - \{1\} \leqslant 0 \\ \qquad \dot{\lambda}^TY = 0 \\ \qquad \dot{\lambda} \geqslant 0 \\ \qquad 0 \leqslant \mu \leqslant \bar{\mu} \\ \qquad 0 \leqslant \Delta \leqslant \bar{\Delta} \end{cases} \tag{37}$$

Here again the sum of increments of plastic multipliers is considered as the objective function to be maximized. In the nonlinear analyses, it is desirable to apply some limitation on the load multiplier and/or nodal displacement. The last two constraints in the MP (37) are considered to limit the load multiplier μ and any nodal displacement Δ to some prescribed load level $\bar{\mu}$ or deflection $\bar{\Delta}$, respectively. As in the usual manner of the proposed RBLP, the above formulated MP is used in the incremental (step-by-step) analysis and the nonlinear constraints (standing for complementarities), $\dot{\lambda}^TY = 0$, are implicitly satisfied at each step. It is worth noting that what is given in Eq. (37) is the initial MP which has to be updated after each plasticity event as described in [18]. In such a way, all problem parameters (including load and plastic multipliers) are decomposed into what has been obtained for the variables up to the current stage of loading (hatted parameters) and an increment which is expected for the next loading step (dotted variables).

$$\begin{aligned} \lambda &= \hat{\lambda} + \dot{\lambda}, \\ \mu &= \hat{\mu} + \dot{\mu} \end{aligned} \tag{38}$$

Accordingly, the initial plastic capacity of the structure (represented by {1} in the initial MP) will decay as loading progresses. Also the MP is updated continuously to obtain correct path and magnitude of the plastic strains (in the space of plastic multipliers) and load amplitude (that causes the next plasticity event) in a single attempt while all extra constraints standing for load/displacement limits are accounted for.

4. Solution procedure

To solve the mathematical programming problem, Eq. (37), a restricted basis linear programming (RBLP) method is employed, as described in [17]. Using this approach, the nonlinear constraints are implicitly accounted for during pivot column selection. Beside this, a special care is taken to detect any possible local unloading. After all, the most important novelty is the proposed maximization

criterion for determining the correct direction of the plastic strain increments in the space of plastic multipliers. This tool, if compared with the classical LCP solution used to begin any new loading step, shows a significantly lower computational effort.

As mentioned before, besides the outstanding features of mathematical programming approaches to nonlinear analysis, the need for large storage space, especially in problems with a huge number of variables, is a drawback that should be managed. Some researchers proposed and used some techniques like partitioning, sifting, and re-meshing. Herein, the required storage space is reduced efficiently by the aid of the revised Simplex method. In addition, a sifting technique is employed which, at each loading step, involves only 4 yield planes that are either active or most likely may become active in the subsequent loading steps. Accordingly, after each load increment, the yield conditions of the whole structure are checked and in the case of any constraint violation, the last load step is disregarded and the selected yield planes are updated. This results in a significant saving in the computational effort and required storage memory. In the following, consistency of the proposed method with the revised Simplex method and the sifting technique are discussed. As described in [17,18], the initial simplex table is decomposed into two adjacent parts; the first part, on the left, is represented by the coefficient matrix $\overline{\mathbf{G}} = \hat{\mathbf{\Phi}}^{\mathbf{T}}\mathbf{\Psi}^{*}_{\sigma}\bar{\boldsymbol{\sigma}}^{\mathbf{v}}\mathbf{\Psi}^{*\mathbf{T}}_{\sigma}\hat{\mathbf{\Phi}} - \mathbf{H}$; the second part, on the right, is indicated by $\underline{\mathbf{G}}$ and reduces to an identity matrix at the beginning; this last matrix is referred to as the "canonical matrix".

4.1. Revised Simplex method

Anytime a pivoting operation is performed in the Simplex table, all the $\overline{\mathbf{G}}$ elements can potentially experience changes, and this represents a large computational effort. Fortunately, the Revised Simplex method [31] permits for avoiding such costly computations by performing the updating of the $\overline{\mathbf{G}}$ matrix only with reference to a specific column (say column j):

$$\bar{\mathbf{G}}^{\mathbf{U}}(:,j) = \underline{\mathbf{G}}\bar{\mathbf{G}}(:,j) \tag{38}$$

where superscript U refers to the updated form of the matrix and colon (:) means all matrix rows. In such a way, instead of updating and keeping the whole matrix $\overline{\mathbf{G}}$, only the required column is updated and used in the process of pivot finding. On the other hand, only few columns of the canonical matrix $\underline{\mathbf{G}}$, specifically those corresponding to the active plastic multipliers, will experience a change due to pivoting and will assume nonzero off-diagonal elements. Accordingly, the required storage space will be efficiently decreased by the aid of a sparse technique.

Beside the above peculiarities, any required column $\bar{\mathbf{G}}(:,j)$ can be computed using only the pertinent rows of the yield matrix and the corresponding columns of the influence and hardening matrices. This represents an additional efficiency in the solution technique, that lets the algorithm to work without building and storing the whole $\overline{\mathbf{G}}$ matrix.

4.2. Sifting technique

In order to avoid the involvement of a huge number of unknowns in the problem formulation, the MP is constructed using the reduced yield matrix of Gauss points. To this end, only 4 yield planes for each Gauss point are used in the MP formulation and, as a consequence, it happens to find some non-participating yield conditions violated during the solution process. In such cases, the most recent pivoting step must be disregarded and the violated yield planes have to be included in the MP formulation. For each pertinent Gauss point, this is simply done by replacing some non-active yield planes with the violated yield planes in the reduced yield matrix. After such substitution, the row in $\overline{\mathbf{G}}$ that corresponds to the modified yield plane, say row j, has to be updated using the following formula:

$$\underline{\mathbf{G}}^{U}(j,\mathrm{V}) = -\overline{\mathbf{G}}(j,\mathrm{V})\underline{\mathbf{G}}(\mathrm{V},\mathrm{V}) \tag{39}$$

where V is a vector containing the row number of all active constraints in the Simplex table and the superscript U still recalls the updated form of the matrix. By the aid of such updating schema, the simplex table will always represent the latest status of the structure and no error can enter into the computed response as a result of yield condition violations; in addition, the proposed method can handle also non-holonomic solutions (see [17]).

5. Numerical examples

In order to verify the proposed maximization criterion and to assess the accuracy of the proposed piece-wise linearization of the yield surfaces, some classic engineering problems are solved. In all problems, the von Mises yield surface is piecewise-linearized using ξ = [0, ±0.5, ±1, ±1.2, ±1.7, ±1.9, ±2] and M = 40, which results in 442 yield planes. Also a piecewise-linear yield model, proposed in [20], with M = 40 (i.e. 120 yield planes) is employed to examine the proposed method for Tresca material model.

Regardless of the employed yield criterion and according to the proposed sifting technique, at each Gauss point only 4 yield planes having the most activation potential are used in the formulation and are updated during the solution process. The important loading stages are determined using the proposed method and are compared to the analytical solutions or to the numerical results available in the literature.

All analyses have been performed on a laptop (*msi* GE620, Intel Core i7-2630QM with 8-GB RAM and Win7 operating system) using a code developed in MATLAB environment.

5.1. Example 1. Plane strain biaxial tension

The first analyzed problem is a very simple element under biaxial tensile stresses in plane strain conditions, as shown in Fig. 3. The structural element properties are as follows: thickness t = 1, elasticity modulus E = 100, Poisson's ratio v = 0.25, and yield stress σ_0 = 1.

According to the double symmetry, only a quarter of the structure is modeled using an 8-noded quadrilateral plane strain element and proper boundary conditions are attributed to fictitious boundaries. However the total number of yield planes for such an element is 442, but by the aid of proposed sifting technique the relevant MP is constructed with only 16 plastic multipliers. The problem is formulated using the von Mises constitutive law in perfect plasticity and in order to capture the structural collapse,

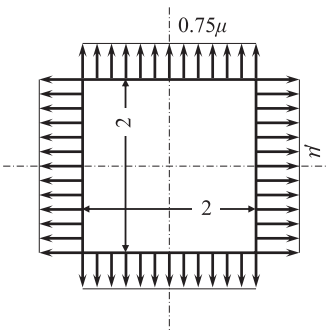

Fig. 3. Biaxial tension test.

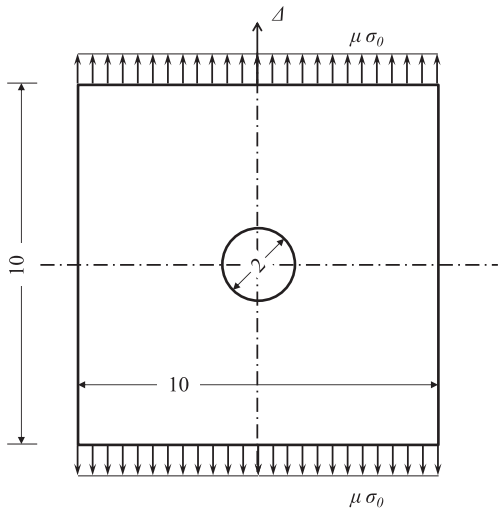

Fig. 4. Perforated square under tensile stress.

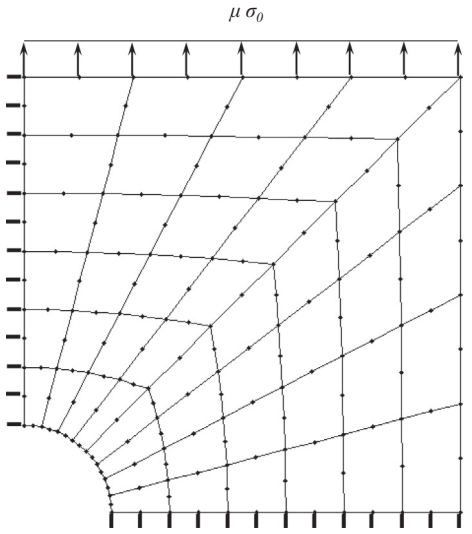

Fig. 5. Finite element domain discretization and shear-free boundary conditions (thick lines represent constrained direction).

the horizontal deflection of the upper-right corner is limited to 0.1. Following the proposed algorithm, the limit load is determined to be μ = 4.6188 which exactly matches the analytical collapse value reported in [32].

5.2. Example 2. Perforated square

The perforated square shown in Fig. 4 is considered as the second example: a 10 × 10 sheet with a D = 2 hole at the center, loaded by tensile stresses on opposite edges. This problem is challenging because of stress concentration and diverse yield mode activations, i.e. tensile yield at the early stages of loading and combinations of normal and shearing yield modes in ultimate load level. The plate is assumed to be in plane stress conditions, with thickness t = 1, and the material mechanical properties are supposed to be as follows: elasticity modulus $E = 10^4$, Poisson's ratio ν = 0.25. Also isotropic elastoplastic material constitutive models, i.e. $\mathbf{H} = \mathbf{0}$, are assumed according to: (a) Tresca classical yield model with c = 0.5 and (b) von Mises model with yield stress σ_0 = 1. The upward displacement Δ is limited to 0.005 as an analysis termination criterion.

Using symmetry advantages, only top-right quarter of the structure is modeled and a shear-free support condition is attributed to the fictitious boundaries. The extracted domain is discretized using 48 × Q8 elements as in Fig. 5. MP for this problem includes 768 plastic multipliers beside the load multiplier as unknowns.

The problem is formulated and solved using the proposed algorithm. The important observations are as follows: for Tresca yield model, the first yielding was detected at the load level μ = 0.390 and the ultimate load corresponding to maximum displacement turns out to be μ = 0.791. The CPU time spent to solve this problem was 107 s, including 1s spent for 9 infeasible load steps and updat-ing the initially selected set of yield planes.

Using the von Mises material model, it is observed that plastic-ity initiates at the load level μ = 0.409 and the procedure terminates at the load level μ = 0.804, at which the upper limit of displacement $\Delta = 0.005$ is reached. The CPU time allocated for this analysis was 59 s, including 1 s spent for revising the initially selected set of yield planes caused by 7 infeasible load steps.

Analytic limit load μ = 0.8 can be easily computed for this problem (see e.g. [33]), which indicates about 1% and 0.6% error in the limit loads predicted for Tresca and von Mises material models, respectively.

The maps of the total dissipated energy are displayed on the structural deformed shapes in Fig. 6 for both constitutive models. As it can be seen, an intensive plastic work is localized at the hole's

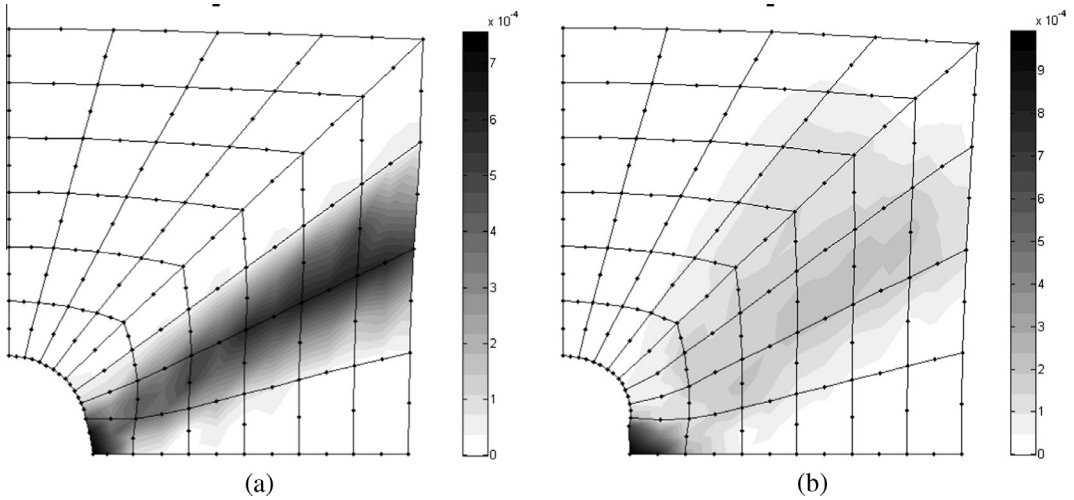

Fig. 6. Dissipated energy map and deformed shape at the ultimate load for (a) von Mises, and (b) Tresca models.

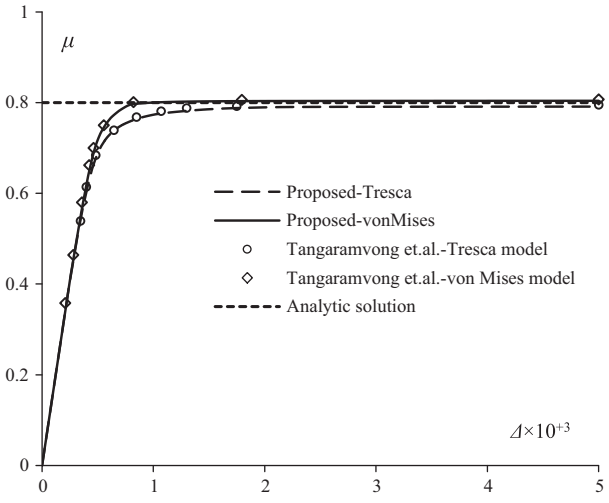

Fig. 7. Load–displacement results for perforated square .

right side, known as normal stress concentration zone, and afterward slip planes started to appear, and the consequent necking caused the failure.

The same problem has been solved in [21] using 120 × Q4 elements with the following results for Tresca/von Mises material models: plasticity initiation load levels 0.345/0.360; limit loads 0.795/0.807; and CPU time 3680/181 s. Also the CPU time wasted for infeasible load levels estimation is reported as 3014/82 s. Fig. 7 compares the obtained load–displacement diagrams to the analytic solution and to the results given in [21]. According to the computed deformed shape, Fig. 6a and b, it appears that a longer specimen would be required to get a better matching with the analytic solution.

5.3. Example 3. Prandtl's punch problem

The flexible flat strip in Fig. 8a resting on an elastoplastic half-space, known as Prandtl's punch problem, is considered as the third example. This problem is frequently studied in the literature and is challenging because of strong stress discontinuities occur-ring in the base material located at the footing corners [34]. A 2×8 rectangular portion of the half space is considered and shear-free and fixed boundary conditions are attributed to the fic-titious boundaries. Also symmetry is exploited to reduce the size of problem and deal with less number of variables, Fig. 8b. For such a domain discretization, the relevant MP includes 1152 plastic multipliers beside the load multiplier as unknowns.

Isotropic elastic-perfectly plastic constitutive behavior is assumed according to: (a) Tresca classical model with cohesion $c = 1$, and (b) von Mises with yield limit $\sigma_0 = 2$. Young modulus $E = 10^4$ and Poisson ratio $\nu = 0.25$ are attributed to the base material and the whole domain is discretized using 72 quadratic quadrilateral elements. The maximum allowable settlement beneath the footing is limited to 0.005. By employing the proposed method, the following results are observed.

For Tresca model, yielding initiates at the load level $\mu = 2.434$ and the limit load corresponding to the allowable settlement 0.005 turns out to be $\mu = 5.171$. The predicted collapse load is in good agreement (0.6% error) with the analytic collapse load $\mu = 5.142$ reported in [34]. The spent CPU time for this problem was 633s which includes 10s that was spent for discarding 24 infeasible load increments and required yield planes updating.

For the von Mises model, yielding initiates at the load level $\mu = 2.657$ and the limit load is predicted to be $\mu = 5.970$. As it was expected, the von Mises yield criterion resulted in a higher limit load than the Tresca model. The CPU time allocated for this case was 951 s including 12 s for cancelling 22 infeasible pivoting and revising preselected set of yield planes.

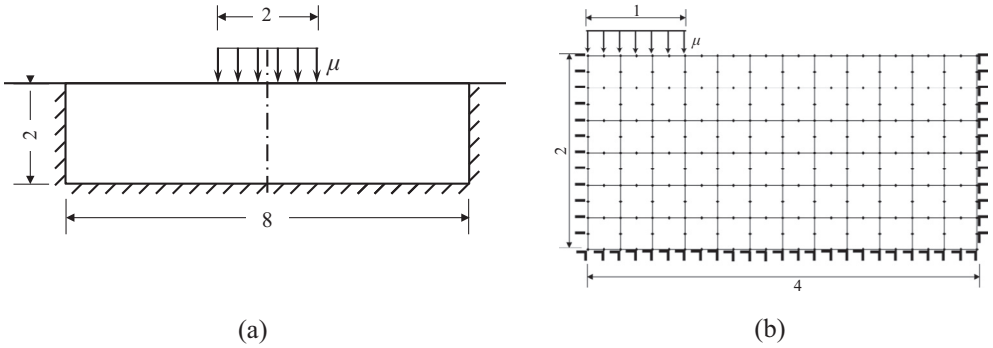

Fig. 8. Prandtl's punch: (a) geometry, and (b) adopted domain and finite element mesh. Thick lines correspond to constrained directions.

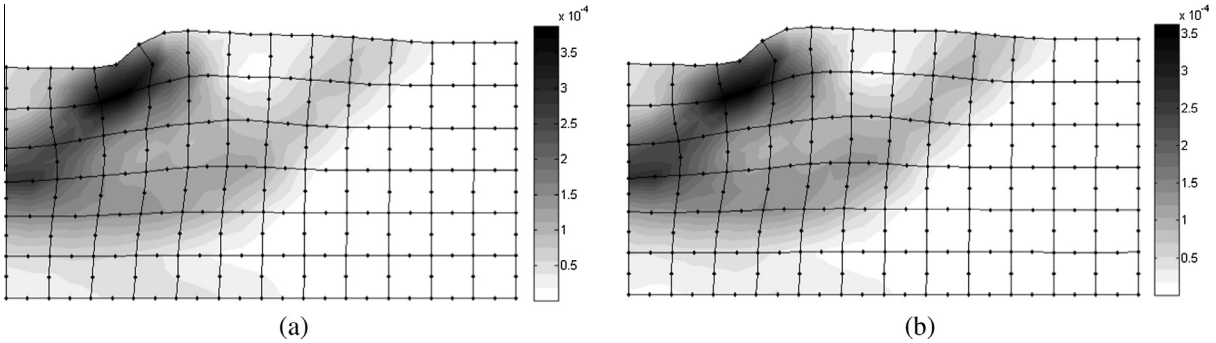

Fig. 9. (a) Dissipated energy map and deformed shape in the ultimate load for Tresca model; (b) the same as (a) but for von Mises material model.

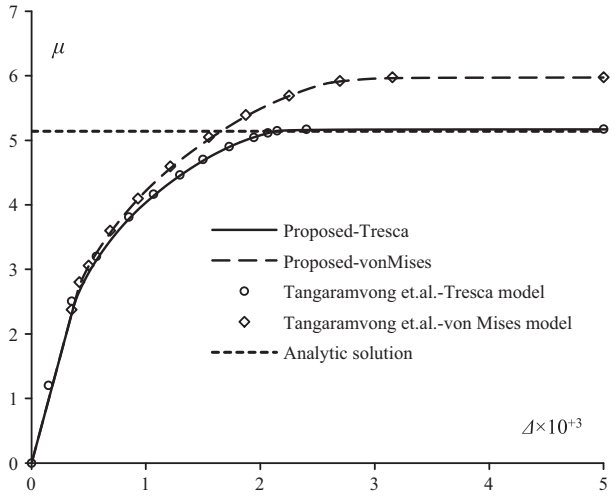

Fig. 10. Load–displacement response of Prandtl's punch problem.

Dissipated energy maps together with the deformed shape at the limit load level are shown in Fig. 9a and b. As expected, intensive plastic deformations are concentrated at the footing corner, and the shear failure zones in the material are clearly depicted by the plastic works.

In Ref. [21], 128 × Q4 elements have been used for discretizing the problem domain, to obtain the following results for Tresca/von Mises models, respectively: plasticity initiation load level 2.390/2.603; limit load 5.174/5.975; and CPU time 4686/415 s. Also 3210/113 s have been wasted for calculation of the load levels beyond the limit load. Plots of load amplifier vs. vertical displacement (measured along the symmetry axis) and analytic solution, for Tresca model, are compared in Fig. 10.

5.4. Example 4. Cook's problem

A non-prismatic solid in plane strain conditions, clamped at one end and loaded by a parabolic tangential stress distribution at the other end, is considered as the final example, Fig. 11a. This problem, known as Cook's problem, is a benchmark problem to examine

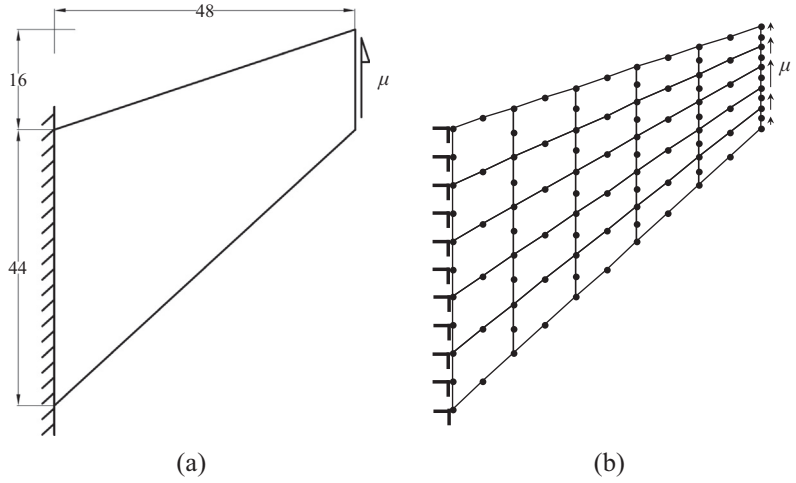

Fig. 11. Cook's problem: (a) geometry and loading layout, (b) finite element mesh.

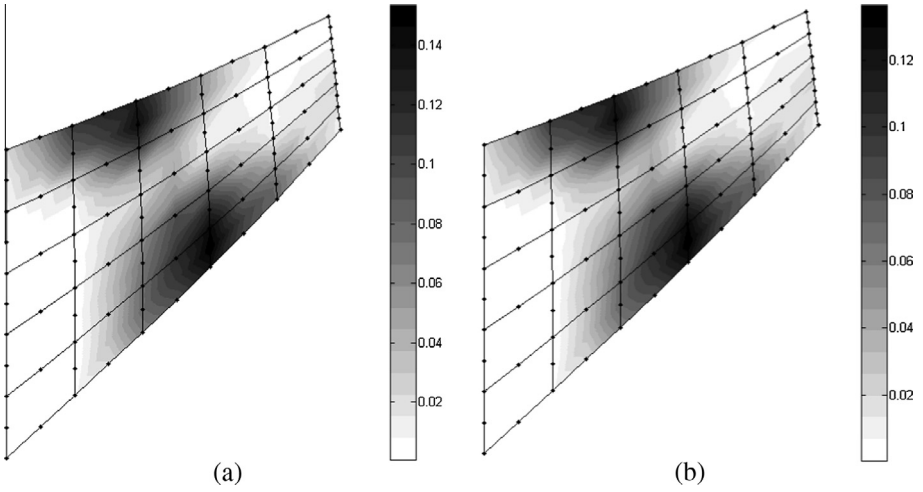

Fig. 12. Cook problem: (a) dissipated energy map on deformed shape for Tresca model, and (b) the same as (a) but for von Mises yield model.

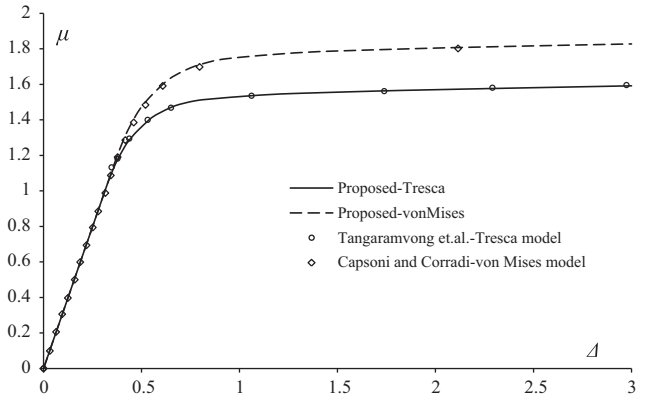

Fig. 13. Results for the Cook's problem.

analysis approaches in dealing with non-uniform meshes. Material properties are $E = 70$, $\nu = 1/3$, $\sigma_0 = 0.243$ and a mixed hardening rule with $h_k = 0.135$ and $h_i = 0.015$ is considered (see e.g. [21,23]). For this example there is no analytical solution available in the literature. As shown in Fig. 11b, the structure is meshed using $25 \times$ Q8 elements and fixed boundary condition is attributed onto support nodes. For this problem a mathematical programming containing 400 plastic multipliers and a load multiplier has to be solved.

The upward displacement of the free end is limited to 3 and the problem is formulated using the proposed algorithm. Results for this problem are as follows: for Tresca material model, the proposed algorithm returned 1.010 and 1.591 as the load levels corresponding to plasticity initiation and imposed limit deflection, respectively. The CPU time in this case did not exceed 4 s.

For von Mises material model, the first yielding was indicated at the load level $\mu = 1.149$ and the upward deflection limit reached at the load level $\mu = 1.828$. For this analysis the CPU time was 9 s.

Also the CPU times spent for yield plane updating in this example for Tresca and von Mises models were 0.08 s and 0.31 s, respectively. In [21], with a mesh of $68 \times$ Q4 elements, the following results are given for Tresca/von Mises material models, respectively: $\underline{\mu} = 0.919/1.031$ as plasticity initiation load level, $\mu = 1.596/1.833$ $\Delta = 3$ and 58/40 s as CPU time.

In Fig. 12, the dissipated energy map is displayed on the deformed shape at the collapse load level. The computed load displacement curves are compared with those taken from [21,23] in Fig. 13.

Here, again, it is seen that the proposed method produced sufficiently accurate results by using a coarser mesh and spending relatively lower CPU times.

6. Conclusion

The use of mathematical programming in 2D-stress/strain nonlinear analysis of structures, which has been considered before in holonomic plasticity, was reconsidered here exploring for non-holonomic solutions. The well-known von Mises criterion was linearized in a single mathematical expression with adjustable number of subdivisions in transversal and radial directions. The outcomes of this research can be summarized as follows:

- The proposed PWL yield surface, which represents an envelope to the original one, was found in satisfactory accuracy with suitably selected number of subdivisions.
- The RBLP method, whose versatility and robustness in frame PWL elastoplasticity has been shown in previous papers (see e.g. [17]), was extended successfully to 2D-stress/strain problems.
- The proposed maximization criterion was proved to serve efficiently in detecting the correct direction of the plastic strain increments at all solution stages, especially in the case of reaching yield surface corners.
- Excluding the round-off errors and those appearing due to piecewise linearization of the yield surface and field discretization, the proposed algorithm follows an exact solution scheme and is capable of capturing any unloading during solution and returning non-holonomic solutions.
- The proposed algorithm benefits the distinct features of a step-by-step algorithm, i.e. stability and exactness, in a more efficient way and produces reliable results.
- Combination of the proposed PWL yield surface and the proposed sifting technique, in which only the yield planes in the vicinity of the stress point are contributed in formulation, provides significant efficiency and savings in computational effort.
- No load step is needed to be pre-assigned. This feature removes any uncertainty regarding solution accuracy and also makes the proposed method capable of capturing the collapse loads robustly.
- The use of quadratic elements with mixed formulation enables the solvers of this kind to return sufficiently accurate results with relatively coarse meshes and, of course, lower computational effort. As mentioned before, all examples have been solved using a non-compiled code developed in MATLAB software, which is known to be relatively slower than the other coding languages such as FORTRAN. However the resulted CPU times in the current version are comparable to the similar methods, the performance of the proposed method in the sense of CPU time could be significantly improved by employing an optimized FORTRAN code.
- The proposed sifting technique works very efficiently and, in all studied examples, it is observed that only a negligible fraction of the total CPU time is spent for cancelling infeasible load steps and revising the working yield planes. Accordingly, by following the proposed algorithm, the majority of the CPU time is devoted to the computing of the unique response path of the structure and the wasted CPU time is not really a matter of concern.

References

[1] Crisfield MA. Non-linear finite element analysis of solids and structures. Essentials, vol. 1. Baffins Lane, Chichester, West Sussex PO19 IUD, England: John Wiley & Sons; 1997.
[2] Crisfield MA. Non-linear finite element analysis of solids and structures. Advanced topics, vol. 2. Baffins Lane, Chichester, West Sussex PO19 IUD, England: John Wiley & Sons; 1997.
[3] Zienkiewicz OC, Taylor RL. The finite element method. sixth ed. Oxford: Butterworth-Heinemann; 2005.
[4] Maier G, Nappi A. On the unified framework provided by mathematical programming to plasticity. In: Dvorak GJ, Shields RT, editors. Mechanics of materials behaviour. Amsterdam: Elsevier; 1983. p. 253–73.
[5] Jirasek M, Bazant ZP. Inelastic analysis of structures. Chichester, UK: Wiley; 2002.
[6] Maier G. A quadratic programming approach for certain classes of non-linear structural problems. Meccanica 1968;3:121–30.
[7] Maier G. Quadratic programming and theory of elastic-perfectly plastic structures. Meccanica 1968;3:265–73.
[8] Maier G. A matrix structural theory of piecewise-linear plasticity with interacting yield planes. Meccanica 1970;5:55–66.
[9] Maier G, Giacomini S, Paterlini F. Combined elastoplastic and limit analysis via restricted basis linear programming. Comput Method Appl Mech Eng 1978;19:21–48.
[10] Giambanco F. Elastic plastic analysis by the asymptotic pivoting method. Comput Struct 1999;71:215–38.
[11] Maier G, Carvelli V, Cocchetti G. On direct methods for shakedown and limit analysis. Eur J Mech A/Solids 2000;19:S79–S100.

[12] Cocchetti G, Maier G. Elastic–plastic and limit-state analyses of frames with softening plastic-hinge models by mathematical programming. Int J Solids Struct 2003;40:7219–44.
[13] Tangaramvong S, Tin-Loi F. Simultaneous ultimate load and deformation analysis of strain softening frames under combined stresses. Eng Struct 2008;30:664–74.
[14] Maier G. Piecewise linearization of yield criteria in structural plasticity. Solid Mech Arch 1976;2:239–81.
[15] Hodge Jr PG. Automatic piecewise linearization in ideal plasticity. Comput Method Appl Mech Eng 1977;10:249–72.
[16] Tin-Loi F. A yield surface linearization procedure in limit analysis. Mech Struct Mach 1990;18:135–49.
[17] Mahini MR, Moharrami H, Cocchetti G. A dissipated energy maximization approach to elastic-perfectly plastic analysis of planar frames. Arch Mech 2013;65:171–94.
[18] Mahini MR, Moharrami H, Cocchetti G. Elastoplastic analysis of frames composed of softening materials by restricted basis linear programming. Comput Struct 2014;131:98–108.
[19] Kaliszky S, Lógó J. Nonlinear analysis of plane problems by mathematical programming. Period Polytech-Civ Eng 1994;38:399–413.
[20] Ardito R, Cocchetti G, Maier G. On structural safety assessment by load factor maximization in piecewise linear plasticity. Eur J Mech A/Solids 2008;27:859–81.
[21] Tangaramvong S, Tin-Loi F, Song Ch. A direct complementarity approach for the elastoplastic analysis of plane stress and plane strain structures. Int J Numer Methods Eng 2012;90:838–66.
[22] Capsoni A, Corradi L. A mixed finite element model for plane strain elastic–plastic analysis. Part I: formulation and assessment of the overall behavior. Comput Method Appl Mech Eng 1997;141:67–79.
[23] Capsoni A, Corradi L. A mixed finite element model for plane strain elastic–plastic analysis. Part II: application to the 4-node bilinear element. Comput Method Appl Mech Eng 1997;141:81–93.
[24] Nagtegaal IC, Parks DM, Rice JR. On numerically accurate finite element solutions in the fully plastic range. Comput Method Appl Mech Eng 1974;4:153–77.
[25] Comi C, Maier G, Perego U. Generalized variable finite element modeling and extremum theorems in stepwise holonomic elastoplasticity with internal variables. Comput Method Appl Mech Eng 1992;96:213–37.
[26] Comi C, Perego U. A unified approach for variationally consistent finite elements in elastoplasticity. Comput Method Appl Mech Eng 1995;121:323–44.
[27] Cocchetti G, Maier G. Static shakedown theorems in piecewise linearized poroplasticity. Arch Appl Mech 1998;68:651–61.
[28] Lubliner J. Plasticity theory. New York: McMillan Publisher; 1990.
[29] Chen WF, Han DJ. Plasticity for structural engineers. New York: Springer-Verlag; 1988.
[30] Capsoni A, Corradi L. A plane strain formulation of the elastic-plastic constitutive law for hardening von Mises materials. Int J Solids Struct 1995;32:3515–31.
[31] Gass SI. Linear programming methods and applications. 4th ed. New York, NY: McGraw-Hill; 1975.
[32] Corradi L, Gioda G. Plane-strain formulation of elastic–plastic constitutive laws. Mech Des Struct Mach 1979;7:325–64.
[33] Vicente da Silva M, Antão AN. A non-linear programming method approach for upper bound limit analysis. Int J Numer Methods Eng 2007;72:1192–218.
[34] Kaliszky S. Plasticity: theory and engineering applications. Amsterdam: Elsevier; 1989.